HHS Public Access

Author manuscript

Nat Neurosci. Author manuscript; available in PMC 2015 September 01.

Published in final edited form as:

Nat Neurosci. 2015 March ; 18(3): 386–392. doi:10.1038/nn.3945.

Dopaminergic and glutamatergic microdomains within a subset of rodent mesoaccumbens axons

Shiliang Zhang[1], **Jia Qi**[1], **Xueping Li**[1,4], **Hui-Ling Wang**[1], **Jonathan P. Britt**[2,5], **Alexander F. Hoffman**[3], **Antonello Bonci**[2], **Carl R. Lupica**[3], and **Marisela Morales**[1,*]

[1]National Institute on Drug Abuse, Neuronal Networks Section, US National Institutes of Health, Baltimore, Maryland, USA

[2]National Institute on Drug Abuse, Synaptic Plasticity Section, US National Institutes of Health, Baltimore, Maryland, USA

[3]National Institute on Drug Abuse, Electrophysiology Research Section, US National Institutes of Health, Baltimore, Maryland, USA

Abstract

Mesoaccumbens fibers are thought to co-release dopamine and glutamate. However, the mechanism of co-release of dopamine and glutamate is unclear, and the co-release by mesoaccumbens fibers has not been documented. By electron microcopy we showed that some mesoaccumbens fibers have vesicular transporters for dopamine (VMAT2) in axon-segments continuous with axon-terminals that lack VMAT2, but contain vesicular glutamate transporters type 2 (VGluT2). *In vivo* overexpression of VMAT2 did not change segregation of the two vesicular types, suggesting highly regulated mechanisms for maintaining this segregation. The mesoaccumbens axon terminals containing VGluT2-vesicles make asymmetric synapses; commonly associated with excitatory signaling. By optogenetics, we showed release of dopamine and glutamate from mesoaccumbens fibers. These findings reveal a complex type of signaling by mesoaccumbens fibers in which dopamine and glutamate although can be released from the same axons; they are not normally released at the same site or from the same synaptic vesicles.

[*]**Correspondence**: Marisela Morales. National Institute on Drug Abuse. Intramural Research Program. Neuronal Networks Section. 251 Bayview Boulevard, Baltimore, MD 21224. mmorales@intra.nida.nih.gov.

[4]Current address: Xi'an Medical University, Xi'an, China

[5]Current address: Department of Psychology, McGill University, Montreal, QC, H3A 1B1, Canada.

A Supplementary Methods checklist is available.

AUTHOR CONTRIBUTIONS

M.M. and S.Z. designed the experiments. S.Z., J.Q., X.L., H-L.W., J.P.B., and A.F.H. performed experiments. S.Z., J.Q., X.L., H-L.W., J.P.B., A.F.H., A.B., C.R.L., and M.M. analyzed data.

M.M. wrote the paper with the contribution of all co-authors.

COMPETING FINANCIAL INTERESTS

The authors declare that they do not have any conflicts of interest (financial or otherwise) related to the data presented in this manuscript.

INTRODUCTION

The simple notion of a dopamine pathway projecting from VTA to nAcc has been complicated by several recent findings. Neurons that project from the VTA to nAcc are molecularly diverse, and may release dopamine, glutamate or GABA. In addition, activation of nAcc fibers from neurons expressing the dopamine transporter (DAT) causes glutamate release in nAcc[1, 2]. It has been suggested that VTA dopamine neurons co-release dopamine and glutamate, but anatomical evidence shows that nAcc axons identified by tyrosine hydroxylase immunoreactivity (TH-IR) make only symmetric synapses in nAcc and do not express any of the known vesicular glutamate transporters[3-5]. Thus the structural basis for the proposed co-release of dopamine and glutamate in the nAcc is unclear.

Two sub-classes of VTA neurons expressing VGluT2 mRNA target the rat nAcc[6, 7]. The cell bodies of one of them express VGluT2 mRNA without detectable levels of TH-IR (*VGluT2-only* neurons), whereas the other sub-class of neurons co-express VGluT2 mRNA and TH-IR (*VGluT2-TH* neurons). It is unclear what type of synapses these neurons establish in the nAcc. The detection of VGluT2-mRNA and TH-protein in VTA cell bodies[7, 8] is consistent with earlier *in vitro* electrophysiological studies demonstrating glutamatergic neurotransmission by mesencephalic TH-IR primary cultures, and the hypothesis that dopamine neurons co-release dopamine and glutamate[9, 10]. Optogenetic studies have further demonstrated that the *VGluT2-TH* mesoaccumbens neurons appear to use glutamate as a signaling molecule[1, 2], though whether *VGluT2-TH* neurons release dopamine in brain tissue remains to be demonstrated.

Although recent phenotypic analysis of rat VTA has shown that *VGluT2-TH* neurons contain aromatic acid decarboxylase[11], and thus are capable of synthesizing dopamine, it is unclear whether these neurons have the capacity to co-release dopamine and glutamate from the same or different subcellular neuronal structures. While some findings provide evidence for lack of vesicular co-localization of dopamine and glutamate, others support the idea of vesicular co-existence of dopamine and glutamate. For instance, findings from high resolution imaging of intact brain tissue indicate that TH and VGluT2 are not co-expressed in the same terminals in the nAcc of adult rats[4, 5] or in mice of any age[3]. However, other studies have reported vesicular co-immunoprecipitation of VMAT2 and VGluT2 in nAcc preparations, leading to the hypothesis that in the nAcc vesicular glutamate co-entry has a synergistic effect on vesicular dopamine filling, and that glutamate and dopamine are co-released in the nAcc from the same pool of vesicles[12, 13].

To determine whether dopamine and glutamate share the same axon terminals or vesicles, we examined the ultrastructural, biochemical, and electrophysiological properties of VGluT2-inputs from VTA neurons in the nAcc. We report that the dual *VGluT2-TH* neurons from both rat and mouse have separate ultrastructural domains for the accumulation and release of either dopamine or glutamate. Specifically, VGluT2 from *VGluT2-TH* neurons is present in synaptic vesicles of axon terminals forming asymmetric synapses, whereas VMAT2 or TH-IR are present in only a subset of these neurons. Moreover, VMAT2 and TH-IR are present in adjacent segments that do not overlap with the terminals containing VGluT2 vesicles, and *in vivo* overexpression of VMAT2 does not disrupt the segregation

between VGluT2 and VMAT2. Although nAcc vesicles do not co-express VGluT2 and VMAT2, optogenetic activation of nAcc fibers from VTA *VGluT2-TH* neurons evokes AMPA/NMDA receptor-mediated EPSCs, and also the release of dopamine. We conclude that both *VGluT2-only* and *VGluT2-TH* neurons form *mesoaccumbens glutamatergic pathways* that parallel the well-known *mesoaccumbens dopaminergic pathway*, and that *VGluT2-TH* neurons in the rat as well as in the mouse possess two distinct contiguous domains specialized for either dopamine or glutamate release.

RESULTS AND DISCUSSION

Rat mesoaccumbens axon terminals (ATs) containing VGluT2 establish asymmetric synapses, while those containing TH-IR establish symmetric synapses

We previously showed that two types of putative glutamatergic VTA neurons (expressing VGluT2 mRNA without TH-IR or co-expressing VGluT2 mRNA and TH-IR) innervate the nAcc[7]. Here we determined the type of synapses that these VTA neurons establish in the shell of the nAcc. We tagged axons from the rat VTA by intra-VTA injections of the anterograde tract tracer *Phaseolus vulgaris* leucoagglutinin (PHA-L) or an adeno-associated virus (AAV) encoding mCherry under the CaMKII promoter (Fig. 1a). With both tracers, we found that within the nAcc some ATs from VTA neurons containing VGluT2-immunoreactivity (VGluT2-IR) formed asymmetric synapses on the heads of dendritic spines or dendritic shafts (Fig. 1b). We determined that 96.09 ± 2.70% of the PHA-L positive ATs that established asymmetric synapses co-expressed VGluT2-IR [70 out of 72 ATs; n = 3 rats; $t(2) = 17.07$, $p = 0.0034$; Fig. 1b]. Among the few TH-IR ATs that formed synapses, most of those co-expressing PHA-L formed symmetric synapses (95.24 ± 4.76%; 17 from 18ATs; n = 3 rats; $t(2) = 9.50$, $p = 0.0109$; Fig. 1c). The infrequent detection of TH-IR terminals making synapses has been previously documented[14]. We also observed VGluT2-terminals and TH-terminals lacking PHA-L, indicating that not all mesoaccumbens cells were tagged, and in the case of VGluT2-terminals indicating that some of these terminals do not originate from the VTA. In addition, we found ultrastructural arrangements in which an mCherry-labeled terminal (from a VTA VGluT2 neuron) formed an asymmetric synapse on the head of a dendritic spine that also received a symmetric convergent mCherry input (from a VTA TH-neuron) on the neck of the spine (Fig. 1d-f). The convergence of glutamatergic-inputs and TH-inputs on a single postsynaptic target is well documented[15], and has been proposed as a synaptic arrangement by which midbrain dopamine release modulates excitatory transmission at the level of individual dendritic spines[16]. Prior studies have shown that glutamatergic inputs from different brain areas synapse on nAcc neurons, and proposed to convey different types of reward-related information during goal-directed behavior. However, the contribution of VGluT2-terminals from VTA neurons to behavioral functions of the nAcc remains to be determined.

Subcellular segregation of dopaminergic and glutamatergic signaling by rat VTA neurons

We next explored the possibility that segregation between dopaminergic and glutamatergic signaling may occur within the same axon. We first determined the distribution of TH-IR and VGluT2-IR in serial sections of nAcc from wild type rats, immunolabeled prior to ultrathin sectioning (“pre-embedding” immunolabeling). In this procedure the antigen-

antibody complexes were identified by silver intensified gold or peroxidase reaction. We occasionally observed TH-IR axon segments contiguous with VGluT2-IR ATs (Fig. 2a and Supplementary Fig. 1). In some instances a TH-IR axon segment making a symmetric synapse (within this domain) was contiguous with a VGluT2-IR AT; in this case the axon-terminal established an asymmetric synapse with a dendritic spine (Supplementary Fig. 1). From these findings, we conclude that under normal conditions axons from rat *VGluT2-TH* neurons maintain in the nAcc independent but adjacent cellular compartments containing either TH-protein, or VGluT2-protein, but not both. Thus, the presence of TH-IR and VGluT2-IR within the same axon provides evidence supporting the idea that some *VGluT2-TH* neurons can synthesize dopamine and also sustain dopamine vesicular release[11].

As with TH-detection, DAT was frequently observed in the nAcc. We occasionally detected DAT signal confined to an axon segment continuous with a VGluT2-IR terminal making an asymmetric synapse on the head of a dendritic spine (Fig. 2b). To further characterize the properties of the axon segments adjacent to VGluT2-IR terminals derived from rat *VGluT2-TH* neurons, we determined the specificity of several anti-VMAT2 antibodies. Out of 8 tested anti-VMAT2 antibodies, one showed selectivity for VMAT2 detection (EB06558 antibody; Supplementary Fig. 2), which was used to determine the distribution of VMAT2-IR signal in relation to VGluT2-IR. While we observed numerous VMAT2- or VGluT2-single labeled terminals in the nAcc, we did not find double-labeled ATs that would indicate co-localization of VMAT2 and VGluT2. However, we occasionally observed examples of VMAT2-IR in the axon segment proximal to a VGluT2-IR terminal making an asymmetric synapse on the head of a dendritic spine (Fig. 2c). Because pre-embedding immunolabeling may result in the differential penetration of antibodies, we further evaluated the pattern of VGluT2 and VMAT2 distribution using a “post-embedding” double immunolabeling procedure. In this procedure ultrathin sections of the nAcc shell were probed with antibodies against VGluT2 or VMAT2 and detected with secondary antibodies bound to colloidal gold of two different sizes. In keeping with results from pre-embedding labeling, we found with post-embedding labeling that when present in the same axon, VMAT2-IR was in the axon segment proximal to a VGluT2-IR terminal making an asymmetric synapse on the head of a dendritic spine (Fig. 2d). We determined that 85.48 ± 3.03% of the labeled ATs had VGluT2; 13.37 ± 2.78% had VMAT2, and 1.15 ± 0.40% appeared to co-express VGluT2 and VMAT2 (Fig. 2e). From these findings, we suggest that *VGluT2-TH* neurons have the capability to store glutamate (via VGluT2) and dopamine (via VMAT2) in distinct vesicular populations that are differentially segregated in subcellular compartments within the same axon.

The ultrastructural findings detailed above provide evidence that in the nAcc the storage of dopamine and glutamate takes place in distinct vesicular pools enriched in different axonal micro-domains. However, to discard that our ultrastructural techniques lacked the sensitivity for co-detection of VGluT2 and VMAT2, we next explored the possibility of coexistence of VGluT2 and VMAT2 at the vesicular level by immunolabeling and by co-immunoprecipitation of VGluT2 and VMAT2 from vesicles obtained from rat nAcc synaptomes. After testing several conditions of isolation for synaptic vesicles, we achieved the experimental conditions (see online methods) that allowed the purification of a

homogeneous population of synaptic vesicles, the quality and purity of which were confirmed by electron microscopy analysis (Fig. 3a). By immunolabeling of these isolated synaptic vesicles, we detected two distinct pools of vesicles, those containing VGluT2-IR and those containing VMAT2-IR (Fig. 3b-d). We found that from a total of 560 labeled vesicles, 66.74 ± 4.10% had VGluT2; 31.71 ± 3.99% had VMAT2, and a very small proportions (1.55 ± 0.35%) appeared to co-label for VGluT2 and VMAT2 (Fig. 3e). The lack of coexistence of VGluT2 and VMAT2 at the vesicular level was next confirmed by co-immunoprecipitation of VGluT2 and VMAT2 from the isolated vesicles. Consistent with our ultrastructural findings, protein preparations of vesicles immunoprecipitated with anti-VGluT2 antibodies showed vesicular immunodetection of both VGluT2 and the vesicular marker synaptophysin, but lacked evidence of VMAT2 (Fig. 3f and Supplementary Fig. 3a). Moreover, protein preparations of vesicles immunoprecipitated with anti-VMAT2 antibodies showed vesicular immunodetection of both VMAT2 and synaptophysin, but lacked evidence of VGluT2 (Fig. 3f and Supplementary Fig. 3a). Thus, we conclude that accumulation of dopamine by VMAT2 occurs in vesicles different from those that accumulate glutamate by VGluT2 (Supplementary Fig. 3b). In contrast to our findings, a previous study using enriched membrane preparations from nAcc reported co-immunoprecipitation of VMAT2 and VGluT2[12]. The discrepancy between this earlier work and our present results may be due to major differences in the material used for immunoprecipitation. In our studies, we used purified synaptic vesicles instead of enriched membranes. In addition, we utilized sucrose to avoid organelle disruption, as organelle disruption may result in membrane fusion among different types of membranes. Moreover, we characterized the specificity of the antibodies used for detection of VMAT2 (Supplementary Fig. 2), to reduce the likelihood of nonspecific antigen recognition. Together, our ultrastructural findings are consistent with our molecular findings and do not support the previously proposed hypothesis that dopamine and glutamate are packaged and co-released in the nAcc from the same pool of vesicles[1, 12, 13].

The segregation and retention of glutamate-vesicles and dopamine-vesicles to distinct axonal domains by mesoaccumbens dual *VGluT2-TH* neurons is in clear contrast to the vesicular organization established by recently discovered dual mesohabenular *VGluT2-GABA* neurons[17]. Notably, mesohabenular neurons concentrate both glutamate-vesicles and GABA-vesicles within a single axon-terminal that establishes excitatory and inhibitory synapses[17]. Thus, VTA *VGluT2* neurons are heterogeneous in their molecular composition[6], their ultrastructural properties and signaling mechanisms.

To further validate the detection of subcellular segregation between VGluT2 and VMAT2 within mesoaccumbens axons, we selectively induced *in vivo* overexpression of VMAT2 with the Myc tag at the amino-terminus [VMAT2(Myc)] in dopamine neurons by injecting an AAV vector encoding Cre-inducible VMAT2(Myc) in the VTA of TH::Cre rats (Fig. 4a). By triple immunofluorescence (TH-VMAT2-Myc), we confirmed Myc expression confined to VTA-TH neurons co-expressing VMAT2 (Fig. 4b). In the nAcc, we observed axons with dual VMAT2-Myc immunolabel contiguous with VGluT2-IR terminals (Fig. 4c,d). By 3-D analysis, we found that the vast majority of mesoaccumbens VGluT2-terminals lacked VMAT2-Myc (99.45 ± 0.08%; 8548 out of 8593 ATs) ($t(3) = 527.00$, $p = 0.0001$). In

addition, we confirmed by electron microscopy the ultrastructural presence of VGluT2 in ATs (making asymmetric synapses) that were adjacent to axon segments containing VMAT2 (Fig. 4e) or Myc (Fig. 4f). We determined that the majority of ATs expressing VGluT2 lacked VMAT2 or Myc (98.84 ± 0.64%;160 out of 162 ATs) ($t(3) = 75.94$, $p = 0.0002$). These findings suggest that VMAT2(Myc) overexpression in mesoaccumbens axons from *VGluT2-TH* neurons does not alter the segregation between VGluT2 and VMAT2. Segregation between VGluT2-vesicles and VMAT2-vesicles may be conferred by specific sorting signals determined by selective motifs within each of these transporters, as previously documented for other vesicular transporters[18].

As in the rat, *VGluT2-only* and *VGluT2-TH* neurons establish asymmetric VGluT2-terminals in the mouse nAcc

To determine whether in the mouse, as in the rat, the VGluT2 neurons form asymmetric synapses in the nAcc, and segregate TH-IR and VGluT2-IR within the same axons, we injected into the VTA of TH::Cre or of VGluT2::Cre mice an AAV vector encoding Cre-inducible light-activated channelrhodopsin2 (ChR2) tethered to mCherry (Fig. 5a and Supplementary Fig. 4a, 5a). In the VTA of infected TH::Cre mice (TH-ChR2-mCherry mice, n = 3), we detected mCherry confined to neurons expressing TH-mRNA (Supplementary Fig. 4b-e). From a total of 576 mCherry-IR neurons, 97.85 ± 0.83% co-expressed TH mRNA (Supplementary Fig. 4f), indicating the selective expression of mCherry under the TH-promoter. In addition, we detected co-expression of mCherry and TH-IR in neurons located within the VTA (Fig. 5b), corresponding to the location of dopamine neurons innervating the nAcc[19]. Because VGluT2-protein is undetectable in cell bodies of glutamatergic neurons, we determined the selectivity of mCherry expression under the VGluT2 promoter by the detection of VGluT2 mRNA in mCherry expressing neurons taken from VTA tissue by laser-capture dissection. By qRT-PCR analysis of individual micro-dissected neurons we confirmed the selective expression of mCherry under the VGluT2 promoter (Supplementary Fig. 5b,c). We found that the ultrastructural features of TH- or VGluT2-mesoaccumbens synapses from mice expressing mCherry under the TH promoter (TH-ChR2-mCherry; Supplementary Fig. 6a) or under the VGluT2 promoter (VGluT2-ChR2-mCherry) were indistinguishable; the mCherry terminals making asymmetric synapses contained VGluT2-protein but not TH-protein (Supplementary Fig. 6b), and those making symmetric synapses contained TH-protein, but not VGluT2-protein (Supplementary Fig. 6c). These ultrastructural findings provide evidence that as in the rat, the *VGluT2-TH* neurons make TH-terminals which are distinct from their VGluT2-terminals, and that their postsynaptic targets on dendritic spines are mutually exclusive (Supplementary Fig. 6d). We observed examples in which a single VGluT2-terminal (from TH-ChR2-mCherry mice or VGluT2-ChR2-mCherry mice) established multiple synapses in the nAcc (Supplementary Fig. 6e-g), indicating that a single VGluT2-terminal has the capacity of affecting multiple postsynaptic neurons.

Taking these findings together, we conclude that both types of VTA neurons expressing VGluT2-mRNA (*VGluT2-only* and *VGluT2-TH* neurons) synthesize VGluT2-protein that is incorporated into vesicles in mesoaccumbens terminals and localized to asymmetric

synapses. We also conclude that the mesoaccumbens VGluT2-terminals from either *VGluT2-only* or *VGluT2-TH* neurons share the same ultrastructural features.

As in the rat, there is subcellular segregation of dopaminergic and glutamatergic signaling by mouse VTA neurons

To determine whether the axonal compartmentalization between the VGluT2-IR and TH-IR observed in the rat nAcc was also present in the mouse, we examined by triple immunofluorescence microscopy the cellular distribution of TH-IR and VGluT2-IR with respect to mCherry-IR in the nAcc of TH-ChR2-mCherry mice (Fig. 5c,d). In the nAcc of these mice, we observed VGluT2 terminal-like structures within single mCherry-axons (Fig. 5c). By 3-D reconstruction, we found cases of TH-IR and VGluT2-IR microdomains along some mCherry-axons, without apparent subcellular overlapping between TH-IR and VGluT2-IR (Fig. 5d). We observed a high frequency of mCherry-VGluT2 label varicosities lacking TH-IR (94.63 ± 0.63%; 1507 varicosities out of 1584)($t(3) = 81.65$, $p = 0.0001$). Thus we conclude that the mouse axons from *VGluT2-TH* neurons, as in the rat, maintain cellular compartmentalization between TH-protein and VGluT2-protein in the same axons within the nAcc. In addition to dual VGluT2-TH axons, we observed in the nAcc of TH-ChR2-mCherry mice TH-IR axons without VGluT2-IR (Supplementary Fig. 7a-e). Under 2-D view, TH-IR appears to be present in segments within mCherry-IR axons and axonal-terminals (Supplementary Fig. 7b). However, the distribution of TH-IR throughout the axon and axon-terminals is better seen after 3-D reconstruction (Supplementary Fig. 7c). The presence of TH-IR throughout the mCherry-IR axon was confirmed by electron microscopy of serial sections (Supplementary Fig. 7d,e). These findings indicate that axonal micro-domains lacking TH-IR are characteristic of *VGluT2-TH* neurons, but not of TH-only neurons.

To determine whether the genetic manipulation of the TH-gene in TH::Cre mice caused alterations in intra-axonal segregation between TH- and VGluT2-signals, we used VGluT2::Cre mice to drive expression of mCherry under the VGluT2 promoter. As detailed above, mCherry expression under the regulation of the VGluT2 promoter was found in both *VGluT2-only* and *VGluT2-TH* neurons (Supplementary Fig. 5d,e). As in the case of findings from TH::Cre mice, some axons expressing mCherry under the VGluT2 promoter had TH-IR. However, TH-IR was excluded from those terminal-like structures containing VGluT2-IR (Supplementary Fig. 5f,g).

Thus quantitative immunofluorescent findings from both TH::Cre and VGluT2::Cre driver lines, together with the ultrastructural findings from analysis of nAcc in the wild type rat, provide convergent evidence that *VGluT2-TH* neurons synthesize both TH-protein and VGluT2-protein, and segregate them to different micro-domains within the same axon.

nAcc photo-stimulation of VGluT2 afferents from VTA neurons elicits EPSCs and dopamine release

The ultrastructural findings demonstrating that VGluT2-axon terminals from both *VGluT2-only* and *VGluT2-TH* neurons establish asymmetric terminals in the nAcc suggest that these VGluT2 terminals use glutamate as a signaling molecule. To evaluate glutamatergic

signaling by VGluT2 mesoaccumbens terminals, VGluT2-ChR2-mCherry fibers were stimulated using 473 nm light pulses delivered into nAcc slices (Fig. 6a-c). As previously reported, we found by whole-cell recordings of NAcc medium spiny neurons that local photo-stimulation of VGluT2-ChR2-mCherry fibers evokes EPSCs (47 ± 14 pA; n = 16 neurons from 3 mice) that depends on both AMPA and NMDA receptors (AMPA/NMDA ratio 1.9 ± 0.4; n = 5 neurons from 3 mice)[13]. As detailed above, there is electrophysiological evidence indicating that some VTA-TH neurons have the capacity to release glutamate in the nAcc[1, 2]. However, it remains to be determined whether some of the same neurons also release dopamine. Here, we applied fast-scan cyclic voltammetry to evaluate dopamine release by *VGluT2-TH* neurons following photo-stimulation of VGluT2-ChR2-eYFP fibers in nAcc slices. We found that selective photo-stimulation of fibers from VTA VGluT2-expressing neurons evoked nAcc phasic release of dopamine (Fig. 6d-j), which was elevated in response to incremental numbers of light pulses (Fig. 6h), and was significantly reduced by bath application of the VMAT2 inhibitor tetrabenazine (Fig. 6i; p = 0.02 vs control). To determine whether light-evoked dopamine responses from *VGluT2-TH* neurons were dependent on glutamate receptors, we measured dopamine release in the nAcc prior to and following application of the glutamate receptor antagonists NBQX (5μM) and AP-5 (40 μM). These antagonists did not significantly alter light-evoked dopamine signals (Fig. 6j). These findings indicate that dopamine is synthesized, stored via a VMAT2-dependent process, and released directly by mesoaccumbens fibers arising from *VGluT2-TH* neurons.

In summary (Supplementary Fig. 8), we present multiple lines of evidence that the two major classes of identified VTA neurons expressing VGluT2 mRNA (*VGluT2-only* and *VGluT2-TH* neurons[6]) synthesize VGluT2 protein that accumulates in synaptic vesicles within terminals forming asymmetric synapses in the nAcc. In agreement with the view that the nAcc asymmetric synapses are excitatory and usually glutamatergic[5], their selective activation evokes excitatory responses in postsynaptic nAcc neurons. Here we report that mesoaccumbens glutamatergic inputs arising from the VTA could themselves converge on the same postsynaptic target. Our findings also indicate that a single VGluT2 terminal from mesoaccumbens neurons can establish multiple synapses and therefore potentially modulate several neurons within the same brain structure. In addition, we provide direct evidence for dopamine release from mesoaccumbens dual glutamatergic-dopaminergic neurons. Whereas our findings are consistent with the idea that *VGluT2-TH* neurons can release both dopamine and glutamate, our results do not support the hypothesis that axon terminals from these neurons co-release dopamine and glutamate from identical axonal terminals. Rather, our findings indicate that synaptic vesicles that release dopamine or glutamate from mesoaccumbens terminals in both adult rats and adult mice are located in distinct microdomains.

ONLINE METHODS

Animals and surgical procedures

The anterograde tracer Phaseolus vulgaris leucoagglutinin (PHA-L) (2.5% in 0.01 M sodium phosphate buffer, pH 7.8; Vector Labs, Burlingame, CA) was applied iontophoretically into

the ventral tegmental area (VTA) (bregma AP −5.2, ML ±0.8, DV −8.4) of 10 male Sprague-Dawley rats (350-420 g body weight) through a stereotaxically positioned glass micropipette (inner tip diameter 20 μm; 5 μA current, 5 s on/off for 15 min). Viral vector adeno-associated virus (AAV) encoding channelrhodopsin2 (ChR2) tethered to mCherry under the CaM Kinase II promoter (AAV5-CaMKII-ChR2-mCherry, 0.2 μl) was delivered into the VTA by pressure through a glass micropipette attached to a Picospritzer III (Parker Hannifin Corporation, Cleveland, OH). Male tyrosine hydroxylase (TH)::Cre mice (The Jackson Laboratory) or vesicular glutamate transporter 2 (VGluT2)::Cre mice (from Dr. Ole Kiehn) (background: C57BL/6 J mouse, 25-30 g body weight[20]) were injected into the VTA with Cre-inducible recombinant AAV encoding ChR2 tethered to mCherry (TH-ChR2-mCherry mice or VGluT2-ChR2-mCherry mice). Male TH::Cre rats (from Dr. Karl Deisseroth, 350-420 g body weight[21]) were injected into the VTA with Cre-inducible recombinant AAV encoding VMAT2 inserted with Myc (Myc epitope was inserted in the N-terminus of VMAT2) [TH-VMAT2(Myc) rats]. Rats or mice were anesthetized with isoflurane (Butler Schein, Dublin, OH) and fixed in a stereotaxic apparatus (David Kopf Instruments, Tujunga, CA) for viral injections. The AAV5-DIO-ChR2-mCherry viral vector [AAV-EF1a-DIO-hChR2(H134R)-mCherry-WPRE-pA; 3×10^{12} genomes/ml] from the UNC Vector Core Facility (Chapel Hill, NC) was injected into the VTA of TH::Cre mice (0.4 μl) or VTA of VGluT2::Cre mice (0.2 μl). The viral vector pAAV-EF1a-DIO-VMAT2(Myc)-WPRE-pA from the Optogenetics and Transgenic Technology Core (NIDA/IRP, Baltimore, MD) was injected into the VTA of TH::Cre rats (0.4 μl; 0.1 μl/min). Each injection was bilaterally with a NanoFil syringe (with 35 gauge needle; WPI, Sarasota, FL) into the VTA (bregma AP −3.4, ML ±0.2, DV −4.3 for mice; bregma AP −5.2, ML ±0.8, DV – 8.4 for rats). The micropipette was left in place for an additional 10 min after each injection. The tracer (PHA-L rats; 2 weeks after injection) and viral injected animals [TH-ChR2-mCherry mice, VGluT2-ChR2-mCherry mice and TH-VMAT2(Myc) rats; 6-8 weeks after injections] were used for anatomical, electrophysiological or electrochemical studies. Rats were double housed, and all mice were housed in groups of up to four animals per cage in the animal rooms. Rats and mice were housed in the animal rooms at 22°C under a 12 h light/dark cycle (light on at 7 am), with ad libitum access to food and water.

For anatomical studies, Sprague-Dawley rats without any manipulation, PHA-L rats, TH-ChR2-mCherry mice, VGluT2-ChR2-mCherry mice and TH-VMAT2(Myc) rats were deeply anesthetized with chloral hydrate (35 mg/100 g), and perfused transcardially with 4% paraformaldehyde (PFA) with 0.15% glutaraldehyde and 15% picric acid in 0.1 M phosphate buffer (PB, pH 7.3). Brains were left in this fixative solution for 2 h at 4°C, solution was replaced with 2% PFA and left overnight at 4°C. Brains were rinsed with PB, and cut into coronal serial sections (50 μm thick) with a vibratome (Leica, Vienna, Austria). All animal procedures were approved by the NIDA Animal Care and Use Committee.

Immunolabeling for light microscopy

Every fifth section of the VTA or nucleus accumbens (nAcc) was used to detect PHA-L or mCherry by immunohistochemistry. Sections were rinsed with 0.1 M PB (pH 7.3) and incubated with a blocking solution [4% bovine serum albumin (BSA) in PB supplemented with 0.3% Triton-X-100] for 1 h. Sections were then incubated with either rabbit anti-PHA-

L antibody (AS-2300; Vector Labs, 1:1000 dilution), mouse anti-mCherry antibody (632543; Clontech Laboratories Inc., Mountain View, CA, 1:500 dilution), or mouse anti-Myc antibody (05-724; EMD Millipore, Billerica, MA, 1:500 dilution); in the blocking solution overnight at 4°C. After rinsing in PB, sections were processed with an ABC kit (Vector Labs), and the peroxidase reaction developed with 0.05% 3, 3-diaminobenzidine-4 HCl (DAB) and 0.003% hydrogen peroxide (H_2O_2). The specificity of primary anti-PHA-L or anti-mCherry antibodies was demonstrated by the lack of PHA-L or mCherry immunolabeling in brain sections from rats or mice injected with saline solution without PHA-L, mCherry, or Myc.

Brain tissue electron microscopy

Pre-embedding immunolabeling—Vibratome brain sections were rinsed with 0.1 M PB (pH 7.3), incubated with 1% sodium borohydride in PB for 30 min to inactivate free aldehyde groups, rinsed in PB, and then incubated with blocking solution [1% normal goat serum (NGS), 4% BSA in PB supplemented with 0.02% saponin] for 30 min. Sections were then incubated with primary antibodies as follows: rabbit (Rb)-anti-PHA-L; mouse (Ms)-anti-mCherry; Rb-anti-PHA-L + guinea pig (Gp)-anti-VGluT2; Rb-anti-PHA-L + Ms-anti-TH; Ms-anti-mCherry + Gp-anti-VGluT2; Ms-anti-mCherry + Rb-anti-TH; Rb-anti-TH + Gp-anti-VGluT2; goat (Gt)-anti-VMAT2 + Gp-anti-VGluT2; Gp-anti-DAT + Rb-anti-VGluT2, or Ms-anti-Myc + Gp-anti-VGluT2. All primary antibodies were diluted in PB with 1% NGS and incubations were for 24 h at 4°C, and used at different dilutions: 1:1000 for Rb-anti-PHA-L, Ms-anti-mCherry, Ms-anti-TH (MAB318; EMD Millipore) and Rb-anti-TH (AB152; EMD Millipore); 1:400 for Gp-anti-VGluT2 (VGluT2-GP-Af240-1; Frontier Institute Co. Ltd) and Gp-anti-DAT (DAT-GP-Af720; Frontier Institute); 1:500 for Ms-anti-Myc and 1:250 for Gt-anti-VMAT2 (EB06558). Sections were rinsed and incubated overnight at 4°C in the corresponding secondary antibodies: biotinylated Gt-anti-Rb (PHA-L single labeling), biotinylated Gt-anti-Ms (mCherry single labeling), anti-Ms-IgG-coupled to 1.4-nm gold (2001; Nanoprobes Inc. Stony Brook, NY, 1:100 dilution, Myc detection), biotinylated Gt-anti-Rb (PHA-L detection) + anti-Gp-IgG Fab' fragment coupled to 1.4-nm gold (2055; 1:100 dilution, VGluT2 detection), biotinylated Gt-anti-Rb (PHA-L detection) + anti-Ms-IgG coupled to 1.4-nm gold (TH detection), biotinylated Gt-anti-Ms (mCherry detection) + anti-Gp-IgG Fab' fragment coupled to 1.4-nm gold (VGluT2 detection), biotinylated Gt-anti-Ms (mCherry detection) + anti-Rb-IgG coupled to 1.4-nm gold (2003; TH detection; 1:100), biotinylated Gt-anti-Rb (TH detection) + anti-Gp-IgG Fab' fragment coupled to 1.4-nm gold (VGluT2 detection), biotinylated Gt-anti-Gp (VGluT2 detection) + anti-Rb-IgG coupled to 1.4-nm gold (TH detection), biotinylated Rb-anti-Gt (VMAT2 detection) + anti-Gp-IgG Fab' fragment coupled to 1.4-nm gold (VGluT2 detection), biotinylated Gt-anti-Gp (VGluT2 detection) + anti-Gt-IgG coupled to 1.4-nm gold (2005; 1:100 dilution, VMAT2 detection), biotinylated Gt-anti-Gp (DAT detection) + anti-Rb-IgG coupled to 1.4-nm gold (VGluT2 detection), or biotinylated Gt-anti-Gp (VGluT2 detection) + anti-Ms-IgG coupled to 1.4-nm gold (Myc detection). Sections were rinsed in PB, and then in double-distilled water, followed by silver enhancement of the gold particles with the Nanoprobe Silver Kit. Next, sections were processed with an ABC kit, fixed with 0.5% osmium tetroxide, and contrasted in 1% uranyl acetate. Sections were dehydrated through a series of graded ethanol and with propylene oxide, and flat embedded in Durcupan ACM

epoxy resin (EMS; Fort Washington, PA). Sections of 70 nm were cut from the outer surface of the tissue with an ultramicrotome UC7 (Leica Microsystems Inc., Buffalo Grove, IL), and collected on formvar-coated grids and counterstained with Reynolds lead citrate.

Post-embedding immunolabeling—Vibratome brain sections from the nAcc shell were rinsed with 0.1 M PB (pH 7.3), incubated with 0.25% tannic acid in water, rinsed in water, and contrasted in 2% uranyl acetate (1 h). Sections were dehydrated through a series of graded ethanol, and infiltrated 1:1 volumes of 100% ethanol and 100% LR White (EMS), 1 volume of 100% ethanol: 2 of 100% LR White, and 100% LR White overnight. Resin was polymerized at 60°C and 70 nm thick sections were cut and dried overnight, rinsed with PB containing 0.1% Tween 20 (PB-Tween 20), and incubated with 0.05 M glycine in PB buffer for 15 min. Sections were blocked with 2.5% NGS and 2.5% BSA in PB (1 h), and followed with incubation with Gt-anti-VMAT2 (1:25 dilution). Sections were rinsed and incubated in donkey anti-Gt 12 nm colloidal gold (705-205-147; Jackson Immunoresearch Laboratories Inc., West Grove, PA, 1:20 dilution) for 1 h. After rinsed with PB-Tween 20, sections were fixed with 2% glutaraldehyde in PB for 10 min, and then rinsed with PB-Tween 20, and incubated with the blocking solution for 1 h, incubated with Gp-anti-VGluT2 antibody (1:20 dilution) overnight at 4°C. Sections were rinsed and incubated in anti-Gp 18 nm colloidal gold (706-215-148; Jackson Immunoresearch Laboratories Inc., 1:10 dilution) for 1 h at room temperature. After rinsed with PB-Tween 20, fixed with 2% glutaraldehyde in PB for 10 min, sections were rinsed with PB-Tween 20, double-distilled water, and counterstained with 5% uranyl acetate and lead.

Sections or vesicles on grids (see below) were examined and photographed using a Tecnai G2 12 transmission electron microscope (FEI Company, Hillsboro, OR) equipped with a digital micrograph 3.4 camera (Gatan, Inc., Pleasanton, CA). Specificity of primary antibodies has been previous described[22] (see below for anti-VMAT2 antibodies).

Ultrastructural analysis of brain tissue

Serial ultrathin sections of the VTA (bregma −4.92 mm to −6.48 mm) and nAcc (bregma 2.76 mm to 0.96 mm) from 10 male Sprague-Dawley rats and 4 male TH::Cre rats were analyzed[23]. We also analyzed serial ultrathin sections of the VTA (bregma −2.92 mm to −3.88 mm) and nAcc (bregma 1.94 mm to 0.86 mm)[24] from 4 male TH-ChR2-mCherry mice and 4 male VGluT2-ChR2-mCherry mice. Synaptic contacts were classified according to their morphology and immunolabel, and photographed at a magnification of 6,800-13,000×. The morphological criteria used for identification and classification of cellular components observed in these thin sections were as previously described[25]. Type I synapses, here referred as asymmetric synapses, were defined by the presence of contiguous synaptic vesicles within the presynaptic axon terminal and a thick postsynaptic density (PSD) greater than 40 nm[25]. Type II synapses, here referred as symmetric synapses, were defined by the presence of contiguous synaptic vesicles within the presynaptic axon terminal and a thin PSD[25]. Serial sections were obtained to determine the type of synapse. In the serial sections, a terminal containing greater than 5 immunogold particles were considered as immunopositive terminal. Pictures were adjusted to match contrast and brightness by using Adobe Photoshop (Adobe Systems Incorporated, Seattle, WA). This experiment was

successfully repeated three times. Electron microscopy and confocal analysis quantification occurred blindly. No statistical methods were used to predetermine sample sizes but our sample sizes are similar to those reported in previous publications[22].

Fluorescence microscopy and image analysis

Coronal brain sections (50 μm) from TH-ChR2-mCherry mice (n = 4), VGluT2-ChR2-mCherry mice (n = 4) or TH-VMAT2(Myc) rats (n = 4) were incubated for 1 h in PB supplemented with 4% BSA and 0.3% Triton X-100. Sections were then incubated with cocktails of primary antibodies: Ms-anti-mCherry (1:500) + Gp-anti-VGluT2 (1:500) + Rb-anti-TH (1:500); Ms-anti-Myc (1:500) + Gt-anti-VMAT2 (1:250) + sheep (Sh)-anti-TH (AB1542; EMD Millipore, 1:500); or Ms-anti-Myc + Gt-anti-VMAT2 + Gp-anti-VGluT2 overnight at 4°C. After rinsing, sections were incubated with the corresponding cocktails of donkey-fluorescent secondary antibodies (Jackson Immunoresearch Laboratories Inc., at 1:100 dilution): Alexa-Fluor-488-anti-Gp +Alexa-Fluor-594-anti-Ms + Alexa-Fluor-647-anti-Rb; Alexa-Fluor-488-anti-Gt + Alexa-Fluor-594-anti-Ms + Alexa-Fluor-647-anti-Sh or Alexa-Fluor-488-anti-Gt + Alexa-Fluor-594-anti-Ms + Alexa-Fluor-647-anti-Gp for 2 h at room temperature. After rinsing, sections were mounted with vectashield mounting medium (Vector Labs) on slides. Fluorescent images were collected with Olympus FV1000 Confocal System (Olympus, Center Valley, PA). Images were taken sequentially with different lasers with 100× oil immersion objectives and Z-stacks were collected at 0.2 μm. Imaris microscopy software (Bitplane Inc., South Windsor, CT) was used to analyze Z-stacks of confocal images from 4 TH-ChR2-mCherry mice or 4 TH-VMAT2(Myc) rats (64 × 64 × 10 μm for each image, 8 images of nAcc from each mouse or rat) to obtain 3-D quantification of axon terminals expressing mCherry, VGluT2 or TH for mice; Myc, VMAT2, or VGluT2 for rats. The same confocal images were analyzed with the Amira microscopy software (Visualization Sciences Group, Burlington, MA) to obtain 3-D reconstruction of putative synapses. This experiment was successfully repeated three times. No statistical methods were used to predetermine sample sizes but our sample sizes are similar to those reported in previous publications[30]. All statistical analyses were performed with GraphPad prism 5.

Testing of anti-VMAT2 antibodies in western blots from total protein preparations from rat nAcc or from transfected cells expressing VMAT2(Myc)

Total protein extracts were obtained from individual slices of the rat nAcc and from transfected cells expressing VMAT2(Myc). For nAcc extracts, 500 μl of 1 × RIPA extraction buffer containing protease inhibitor (Roche Applied Science, Penzberg, Germany) was added to nAcc slices. Tissue was homogenized on ice for 30 s, and then centrifuge at 13,200 rpm for 15 min at 4°C. Supernatant was collected, and protein concentration was measured before stored at −20°C. For cellular overexpression of VMAT2, we used the plasmid pAAV-EF1a-DIO-VMAT2-WPRE-pA which was constructed by Tritsch et al.[26] and obtained from Addgene (Cambridge, MA). To this plasmid, a Myc epitope tag was inserted in-frame with VMAT2 at the N-terminus (pAAV-EF1a-DIO-VMAT2(Myc)-WPRE-pA; pOTTC487; see graphic map in Supplementary Figure 1) for immunodetection of transgenic VMAT2. To prepare cell lysates from VMAT2(Myc) overexpressing cells, HEK293 cells were placed in a 24-well plate and transfected the next day using 0.4 μg of pAAV-EF1a-DIO-VMAT2(Myc)-WPRE-pA DNA and 0.4 μg of pAAV-cfos-iCre DNA

(pOTTC230) per well, Lipofectamine 2000 transfection reagent (Life technologies, Grand Island, NY) and Opti-MEM reduced serum medium (31985-062; Life technologies). The pOTTC230 plasmid was constructed by the Optogenetics and Transgenic Technology Core (NIDA/IRP; Baltimore, MD). Cells were harvested 2 days after transfection by adding 100 ul of modified RIPA buffer containing 50 mm Tris-HCl (pH 7.4), 0.25% sodium deoxycholate, 150 mm NaCl, 1 mm EDTA, 1% Nonidet P-40, and 1× protease inhibitor mixture (Sigma Aldrich). The collected samples underwent 3 cycles of rapid freeze-thaw and centrifuged at 12,000 rpm for 10 min at 4°C. Supernatant from centrifuged cell lysates was collected. Protein concentration was measured and stored at −80°C until western blot analysis was performed.

Electrophoretic separation of peptides from total protein nAcc extracts and from cell transfected extracts was done by standard electrophoresis. Western blots of nAcc were probed with the following primary antibodies: Gp-VGluT2 (AB2551; EMD Millipore, 1:5000 dilution); Rb-anti-VMAT2 (ab371945; Abcam, Cambridge, MA); Rb-anti-VMAT2 (Phoenix pharmaceuticals, Inc., 1:500); Rb-anti-VMAT2 (ab81855; Abcam, 1:500); Rb-anti-VMAT2 (VMAT2-Rb-Af720; Frontier Institute Co. Ltd, 1:1000); Rb-anti-VMAT2 (138302; Synaptic Systems, Germany, 1:1000); Rb-anti-VMAT2 (AB1598P; EMD Millipore, 1:1000 dilution); Gt-anti-VMAT2 (SAB2501101; Sigma-Aldrich, St. Louis, MO, 1:1000), and Gt-anti-VMAT2 (EB06558; Everest Biotech, 1:1000). Western blots of cell-transfected extracts were probed with the anti-VMAT2 antibody (EB06558) and anti-Myc antibody (1:1000 dilution) to determine the specificity of the anti-VMAT2 antibody (EB06558). This experiment was successfully repeated three times.

Preparation of synaptic vesicles from nAcc

We tested several experimental conditions to obtain synaptic vesicles, including the method described by Hnasko et al.[12], by following this method, we obtained material that under the electron microscope appeared as aggregates of electron-dense material without recognizable ultrastructure. Among the different tested methods, we found that the one from the groups of Teng et al. and Erickson et al.[27, 28] provided in our hands the best yield of synaptic vesicles, which purity was confirmed by electron microscopy. We used 30-40 male Sprague-Dawley rats (6 weeks of age) for each batch of isolation of synaptic vesicles. The isolation of synaptic vesicles was done 3 times from a total of 110 rats. Rats were deeply anesthetized with chloral hydrate (35 mg/100 g), brains were removed, the nAcc region was dissected out and homogenized in ice-cold 5 mM HEPES buffer (pH 7.4) with 0.32 M sucrose and cocktail of protease inhibitor (Roche Applied Science). For vesicle preparations, materials from 10 rats were processed each time, and all the following steps were performed at 4°C. The homogenate was then centrifuged at 2,000 g for 10 min. The resulting supernatant was centrifuge at 10,000 g for 30 min. The pellet containing the enriched synaptosomal fraction was homogenized for 5 min after adding 1.6 ml of double distilled water containing protease inhibitors. The osmolarity of this preparation was restored by adding 200 μl of 0.25 M potassium HEPES (pH 6.5) and 200 μl of 1.0 M neutral L-(+)-tartaric acid dipotassium salt buffer (pH 7.5). For immuno-gold labeling and electron microscopy analysis, the supernatant was diluted in HEPES/K^+ tartrate to a final concentration of 0.1 M and processed for immuno-gold EM. For co-immunoprecipitation and western blot experiments,

the suspension was centrifuged at 20,000 g for 20 min, the obtained supernatant was then centrifuged at 55,000 g for 60 min. $MgSO_4$ buffer (final concentration 1 mM) was added to the supernatant and followed by a final centrifugation at 100,000 g for 45 min. The pellets containing the isolated synaptic vesicles were resuspended in vesicle assay buffer containing 5 mM HEPES, 0.32 M sucrose, and protease inhibitors. The synaptic vesicles were frozen in liquid nitrogen and stored at −80°C until use. The purity of the synaptic vesicle preparation was determined under the electron microscope. This experiment was successfully repeated three times.

Isolated synaptic vesicles and electron microscopy

Ultrastructural evaluation of isolated synaptic vesicles—The purity of the different batches of isolated synaptic vesicles was evaluated following the method of Kadota and Kadota (1973) with some modification[29]. Pellet harvested in the last step of centrifugation was fixed with 2% OsO_4 for 1 h, briefly rinsed with double-distilled water, and post-fixed with 12% glutaraldehyde in double-distilled water overnight at 4°C. After fixation, the pellet was rinsed with water and stained with 4% uranyl acetate for 30 min, dehydrated in series of graded ethanol, and embedded with Durcupan ACM epoxy resin. Resin-embedded sections were polymerized at 60°C for 2 days. Sections of 70 nm were cut with an ultramicrotome UC7 using a diamond knife. The sections were collected on formvar-coated single slot grids and counterstained with Reynolds lead citrate.

Immuno-gold detection of VGluT2 and VMAT2 within the isolated synaptic vesicles—The presence of VGluT2 and VMAT2 within the synaptic membranes of the isolated vesicles was detected following the method of Boulland et al. with some modification[30]. Synaptic vesicles isolated from the nAcc were diluted with 0.1 M K^+ tartrate/EDTA (1/10, 1/20). Twenty microliters of isolated vesicles were applied onto formvar and carbon coated nickel grids. Following the formation of a film of solution on the surface of the grid, each grid was immediately placed on top of drops of 4% PFA and fixed overnight at 4°C. Grids were rinsed with PB, treated with 1 M ethanolamine-HCl for 10 min, rinsed with PB, blocked for 1 h with 10% newborn calf serum (NCS) in 0.1 M Tris/HCl (pH 7.4)/0.3 M NaCl (TBS), and incubated with the first primary antibody (Gt-anti-VMAT2; 1:25 dilution) diluted with 1% NCS/TBS, overnight at 4°C. After rinsed with 1% NCS/TBS, grids were incubated with the first secondary antibody (donkey anti-goat 12 nm colloidal gold; 705-205-147; 1:20 dilution) in 1% NCS/TBS containing 5 mg/10 ml polyethylene glycol (PEG) for 2 h at room temperature. Grids were rinsed with TBS and fixed with 2.5% glutaraldehyde in PB for 10 min. Grids were rinsed with PB, blocked for 1 h with 1% NCS/TBS, and incubated with the second primary antibody (Gp-anti-VGluT2; 1:20 dilution) diluted with 1% NCS/TBS overnight at 4°C. After rinsed with 1% NCS in TBS, grids were incubated with the second secondary antibody (donkey anti-Gp-18 nm colloidal; 1:10 dilution) in 1% NCS/TBS/PEG for 2 h at room temperature. Grids were rinsed with TBS and fixed with 2.5% glutaraldehyde in PB for 10 min. After rinsed with double-distilled water, grids were fixed with 1% OsO_4 in PB, rinsed with water, and for negative contrast, grids were rinsed with 3 drops of 1% uranyl acetate and immediately dried on filter paper.

Sections or vesicles on grids were examined and photographed using a Tecnai G2 12 transmission electron microscope (FEI Company, Hillsboro, OR) equipped with a digital micrograph 3.4 camera (Gatan, Inc., Pleasanton, CA). Specificity of primary antibodies has been previous described[22] (see above for anti-VMAT2 antibodies).

Co-immunoprecipitation and immunoblotting

For co-immunoprecipitation, primary antibodies were cross-linked to protein A or G-coated Dynabeads using the immunoprecipitation kit that includes "binding & washing buffer" (Life Technologies). Dynabeads were washed in the antibody "binding & washing buffer", and incubated with the corresponding primary antibody (Gp-anti-VGluT2 or Gt-anti-VMAT2) with rotation for 10 min at room temperature. After incubation with each primary antibody, beads were washed with the antibody "binding & washing buffer". Beads with attached antibody were resuspended with synaptic vesicle solution by adding assay buffer containing 5 mM HEPES, 0.32 M sucrose, and 1× protease inhibitors to obtain a final vesicle concentration of 0.1 μg/μl. Incubation was at room temperature for 100 min with rotation. After incubation, the supernatant was transferred to a clean tube for further analysis. The Dynabeads-Antibody-Vesicles complex was washed 4 times by using washing buffer and then the sample was gently resuspended in the elution buffer. Proteins from aliquots of the original synaptic vesicle solution, Dynabeads-Antibody-Vesicles elution, and the above supernatant were separated by standard electrophoresis, and western blots of these samples were probed with the following primary antibodies: Ms-anti-VGluT2 (MAB5504; EMD Millipore, 1:2000), Gt-anti-VMAT2 (EB06558; Everset Biotech, 1:500), and Ms-anti-synaptophysin p38 (MAB638; EMD Millipore, 1:4000). Western blots immunoprobed for VMAT2 were performed using Quick Western Kit (926-68100; LI-COR). This experiment was successfully repeated three times.

Slice preparation for electrophysiology or voltammetry

Six to eight weeks after virus injection, male VGluT2-ChR2-mCherry mice for electrophysiology and male VGluT2-ChR2-eYFP mice for voltammetry were anesthetized with Euthasol and perfused with ice-cold, artificial cerebrospinal fluid (ACSF), saturated with 95% O_2 and 5% CO_2, and modified to contain (in mM): 92 NMDG, 20 HEPES, 25 glucose, 30 $NaHCO_3$, 1.2 NaH_2PO_4, 2.5 KCl, 5 sodium ascorbate, 3 sodium pyruvate, 2 thiourea, 10 $MgSO_4$, 0.5 $CaCl_2$. Brains were then removed quickly, placed in this same solution on a VT-1200 vibratome (Leica, Nussloch, Germany), and sectioned through the nAcc in coronal slices (200 μm thick for electrophysiology or 280 μm thick for voltammetry).

Slice electrophysiology

The slices were placed in a holding chamber filled with the same solution, but held at 32°C ACSF. For recordings, slices were transferred to a chamber superfused 32°C ACSF modified to contain (in mM): 125 NaCl, 2.5 KCl, 1.25 NaH_2PO_4, 1 $MgCl_2$, 2.4 $CaCl_2$, 26 $NaHCO_3$ and 11 glucose. Picrotoxin (100 μM) was included in this solution to block inhibitory transmission. Electrodes (3-5 MΩ) were backfilled with an internal solution containing (in mM): 117 cesium methanesulfonate, 20 HEPES, 0.4 EGTA, 2.8 NaCl, 5 TEA-Cl, 3 QX-314, 4 Mg-ATP and 0.4 Na-GTP (280-285 mOsm). Cells were visualized on

an upright microscope using infrared differential interference contrast video microscopy. Whole-cell voltage-clamp recordings were made using a MultiClamp 700B amplifier (2 kHz low-pass Bessel filter and 10 kHz digitization) with pClamp 10.3 software (Molecular Devices, Sunnyvale, CA). Medium spiny neurons in the nAcc shell identified by morphology, membrane resistance, and resting membrane potential, were voltage clamped at −80 mV, unless otherwise noted. Series resistance (10-25 MΩ) was monitored with a 5 mV hyperpolarizing pulse (50 ms) given every 20 s, and only recordings that remained stable over the period of data collection were used. A 200 μm core optical fiber, coupled to a diode-pumped solid state laser, was positioned just above the slice and aimed at the recorded cell. Optically-evoked EPSCs were obtained every 20 s with paired pulses of 473 nm wavelength light (30 mW, 3 ms) using 50, 100, and 200 ms inter-pulse intervals. AMPA-NMDA receptor response ratios were calculated from EPSCs recorded at both −80 and +40 mV. The AMPAR-mediated portion was obtained by averaging 5 optically-evoked EPSCs recorded at −80 mV. The NMDAR-mediated portion was determined by sampling a 5 ms window, 40 ms after the peak AMPAR-mediated current, in EPSCs recorded at +40 mV. Drugs were obtained from either Sigma or Tocris Bioscience. Neurons were randomly and blindly sampled.

Voltammetric measurements of dopamine release in nAcc slices

Before initiating voltammetric recordings, a single brain slice was submerged in a low-volume (170 μl) recording chamber and continuously bathed with warm (30-32°C) ACSF at 2 ml/min. The aCSF was warmed using an inline solution heater (TC-324B, Warner Instruments, Hamden, CT, USA). Fast-scan cyclic voltammetry (FSCV) was performed using carbon fiber electrodes as described previously[31]. Carbon fibers (7 μm diameter, Goodfellow Corp., Devon, PA, USA) were aspirated into glass micropipettes, which were then pulled using a vertical electrode puller (Kopf Instuments Model 700-D). Carbon fibers were trimmed to allow ~20-50 μm to protrude from the glass capillary. Pipettes containing the carbon fiber were filled with a solution of 4M K-acetate/150 mM KCl and attached to the head stage of a patch clamp amplifier (HEKA EVA-8, HEKA Instruments Inc., Southboro, MA, USA). Voltammetric scans, stimulus wave form generation and timing, and data collection were performed using A/D boards (PCI 6052E and PCI-6711E, National Instruments, Austin, TX, USA) and custom LabView-based software. All carbon fiber electrodes were tested for stable background currents and responsiveness in ACSF containing dopamine (2 μM) prior to and following each experiment.

An epifluorescence-equipped upright microscope (Axioskop-2, Zeiss) was used to visualize areas of high YFP expression for recording within each slice. Carbon fibers were placed at a depth of ~75-100 μm within the nAcc. Optical stimulation was delivered to the slice using published methods[32] via an optical fiber (200 μm core, Thorlabs, Newton, NJ) coupled to a 150 mW, 473 nm diode pumped solid state continuous wave laser system (OEM Laser Systems Salt Lake City, UT). The fiber was placed just above the surface of the slice. Optical stimulation consisted of a varying number of 5 ms duration pulses, delivered at 25 Hz. Laser power was kept at < 2 mW output in all cases. In some slices, dopamine signals were also elicited by electrical stimulation (5-10 V, 5 × 1 ms pulses, 25 Hz) using a conventional bipolar stimulating electrode consisting of formvar-insulated nichrome wire

(50 μm diameter). Voltammetric scans from −0.4 to 1.0 V and back were performed at 400 V/s (7 ms scan duration) at a frequency of 10 Hz. A 5 s background measurement (50 scans) was taken prior to stimulation of the brain slice and subtracted from the voltammetric scan obtained at the signal peak immediately after stimulation. This was used to generate a voltammogram (current vs. voltage plot) for each signal. All signals matched those expected for the oxidation and reduction of dopamine. For experiments involving application of glutamate receptor antagonists, signals were taken every 90 s. After obtaining a stable baseline, NBQX (5 μM) and AP-5 (40 μM) were applied to the slice, and the light-evoked dopamine response was monitored over a 10-15 minute period. Neurons were randomly and blindly sampled. No statistical methods were used to determine these sample sizes in advance, but sample sizes were based on our previous work utilizing within-slice protocols[17, 31, 33]. In all cases, we obtained slices from at least 2 animals to verify the reproducibility of the dataset.

Single cell quantitative RT-PCR of VTA neurons expressing mCherry under the regulation of the VGluT2 promoter

Male adult VGluT2-ChR2-mCherry mice (n = 3, 25-30 g body weight) were anesthetized with chloral hydrate (35 mg/100 g body weight), and perfused transcardially with 10% RNAlater (Ambion, Foster City, CA) in 0.1 M PB, pH 7.4, as previously described[11]. Brains were immediately removed and frozen in isopentane at −40°C. Coronal cryosections were used to obtain VTA mCherry labeled neurons for VGluT2 qRT PCR as previously detailed[34].

Cellular immunodetection of mCherry expressed under the regulation of the TH promoter and its co-expression with TH mRNA

Male TH-mCherry mice (n = 3) were anesthetized with chloral hydrate (35 mg/100 g) and perfused transcardially with 4% PF in PB, pH 7.3. The brains were removed, left in 4% PF for 2 h at 4°C, and transferred to18% sucrose solutions in PB overnight at 4°C. Coronal serial cryosections were processed for dual detection of mCherry immunoreactivity and TH mRNA, as previously detailed.

Statistics analysis

Rats and mice in anatomical, electrophysiological, and voltammetric studies were excluded from data analysis if the injection sites were incorrect. Image collection and analysis were according to the method of randomization. All statistical analyses applied in anatomy studies were performed with GraphPad Prism 5. In 3-D fluorescence microscopy, electron microscopy, and voltammetry studies, we performed paired t-test to analyze data when applicable. Data distribution was assumed to be normal but this was not formally tested. $p < 0.05$ was considered significant.

Supplementary Material

Refer to Web version on PubMed Central for supplementary material.

ACKNOWLEDGEMENTS

The Intramural Research Program of the National Institute on Drug Abuse (IRP/NIDA/NIH) supported this work. The viral packaging and *in vitro* testing of the AAV-DIO-VMAT2(Myc) vector were done by the NIDA IRP Optogenetics and Transgenic Technology Core (OTTC). We thank Drs. Ole Kiehn and Lotta Borgius for providing the VGluT2::Cre transgenic mice, and Dr. Karl Deisseroth for the TH::Cre transgenic rats. Resources for three-dimensional analysis were supported by NS050274.

REFERENCES

1. Stuber GD, Hnasko TS, Britt JP, Edwards RH, Bonci A. Dopaminergic terminals in the nucleus accumbens but not the dorsal striatum corelease glutamate. J Neurosci. 2010; 30:8229–8233. [PubMed: 20554874]
2. Tecuapetla F, et al. Glutamatergic signaling by mesolimbic dopamine neurons in the nucleus accumbens. J Neurosci. 2010; 30:7105–7110. [PubMed: 20484653]
3. Berube-Carriere N, et al. Ultrastructural characterization of the mesostriatal dopamine innervation in mice, including two mouse lines of conditional VGLUT2 knockout in dopamine neurons. Eur J Neurosci. 2012; 35:527–538. [PubMed: 22330100]
4. Berube-Carriere N, et al. The dual dopamine-glutamate phenotype of growing mesencephalic neurons regresses in mature rat brain. J Comp Neurol. 2009; 517:873–891. [PubMed: 19844994]
5. Moss J, Ungless MA, Bolam JP. Dopaminergic axons in different divisions of the adult rat striatal complex do not express vesicular glutamate transporters. Eur J Neurosci. 2011; 33:1205–1211. [PubMed: 21375596]
6. Morales M, Root DH. Glutamate neurons within the midbrain dopamine regions. Neuroscience. 2014; 282C:60–68. [PubMed: 24875175]
7. Yamaguchi T, Wang HL, Li X, Ng TH, Morales M. Mesocorticolimbic glutamatergic pathway. J Neurosci. 2011; 31:8476–8490. [PubMed: 21653852]
8. Kawano M, et al. Particular subpopulations of midbrain and hypothalamic dopamine neurons express vesicular glutamate transporter 2 in the rat brain. J Comp Neurol. 2006; 498:581–592. [PubMed: 16917821]
9. Dal Bo G, et al. Dopamine neurons in culture express VGLUT2 explaining their capacity to release glutamate at synapses in addition to dopamine. J Neurochem. 2004; 88:1398–1405. [PubMed: 15009640]
10. Sulzer D, et al. Dopamine neurons make glutamatergic synapses in vitro. J Neurosci. 1998; 18:4588–4602. [PubMed: 9614234]
11. Li X, Qi J, Yamaguchi T, Wang HL, Morales M. Heterogeneous composition of dopamine neurons of the rat A10 region: molecular evidence for diverse signaling properties. Brain structure & function. 2013; 218:1159–1176. [PubMed: 22926514]
12. Hnasko TS, et al. Vesicular glutamate transport promotes dopamine storage and glutamate corelease in vivo. Neuron. 2010; 65:643–656. [PubMed: 20223200]
13. Hnasko TS, Hjelmstad GO, Fields HL, Edwards RH. Ventral tegmental area glutamate neurons: electrophysiological properties and projections. J Neurosci. 2012; 32:15076–15085. [PubMed: 23100428]
14. Descarries L, Watkins KC, Garcia S, Bosler O, Doucet G. Dual character, asynaptic and synaptic, of the dopamine innervation in adult rat neostriatum: a quantitative autoradiographic and immunocytochemical analysis. J Comp Neurol. 1996; 375:167–186. [PubMed: 8915824]
15. Morales M, Pickel VM. Insights to drug addiction derived from ultrastructural views of the mesocorticolimbic system. Ann N Y Acad Sci. 2012; 1248:71–88. [PubMed: 22171551]
16. Freund TF, Powell JF, Smith AD. Tyrosine hydroxylase-immunoreactive boutons in synaptic contact with identified striatonigral neurons, with particular reference to dendritic spines. Neuroscience. 1984; 13:1189–1215. [PubMed: 6152036]
17. Root DH, et al. Single rodent mesohabenular axons release glutamate and GABA. Nat Neurosci. 2014; 17:1543–1551. [PubMed: 25242304]

18. Foss SM, Li H, Santos MS, Edwards RH, Voglmaier SM. Multiple dileucine-like motifs direct VGLUT1 trafficking. J Neurosci. 2013; 33:10647–10660. [PubMed: 23804088]
19. Swanson LW. The projections of the ventral tegmental area and adjacent regions: a combined fluorescent retrograde tracer and immunofluorescence study in the rat. Brain Res Bull. 1982; 9:321–353. [PubMed: 6816390]
20. Borgius L, Restrepo CE, Leao RN, Saleh N, Kiehn O. A transgenic mouse line for molecular genetic analysis of excitatory glutamatergic neurons. Mol Cell Neurosci. 2010; 45:245–257. [PubMed: 20600924]
21. Witten IB, et al. Recombinase-driver rat lines: tools, techniques, and optogenetic application to dopamine-mediated reinforcement. Neuron. 2011; 72:721–733. [PubMed: 22153370]
22. Tagliaferro P, Morales M. Synapses between corticotropin-releasing factor-containing axon terminals and dopaminergic neurons in the ventral tegmental area are predominantly glutamatergic. J Comp Neurol. 2008; 506:616–626. [PubMed: 18067140]
23. Paxinos, G.; Watson, C. The Rat Brain in Stereotaxic Coordinates. Elsevier; 2007.
24. Paxinos, G.; Franklin, KBJ. The Mouse Brain in Stereotaxic Coordinates. Academic Press; 2001.
25. Peters, A.; Palay, SL.; Webster, H.d. The fine structure of the nervous system: neurons and their supporting cells. Oxford University Press; 1991.
26. Tritsch NX, Ding JB, Sabatini BL. Dopaminergic neurons inhibit striatal output through non-canonical release of GABA. Nature. 2012; 490:262–266. [PubMed: 23034651]
27. Erickson JD, Masserano JM, Barnes EM, Ruth JA, Weiner N. Chloride ion increases [3H]dopamine accumulation by synaptic vesicles purified from rat striatum: inhibition by thiocyanate ion. Brain Res. 1990; 516:155–160. [PubMed: 1694707]
28. Teng L, Crooks PA, Dwoskin LP. Lobeline displaces [3H]dihydrotetrabenazine binding and releases [3H]dopamine from rat striatal synaptic vesicles: comparison with d-amphetamine. J Neurochem. 1998; 71:258–265. [PubMed: 9648873]
29. Kadota K, Kadota T. Isolation of coated vesicles, plain synaptic vesicles, and flocculent material from a crude synaptosome fraction of guinea pig whole brain. J Cell Biol. 1973; 58:135–151. [PubMed: 4125368]
30. Boulland JL, et al. Vesicular glutamate and GABA transporters sort to distinct sets of vesicles in a population of presynaptic terminals. Cereb Cortex. 2009; 19:241–248. [PubMed: 18502731]
31. Good CH, et al. Impaired nigrostriatal function precedes behavioral deficits in a genetic mitochondrial model of Parkinson's disease. Faseb J. 2011; 25:1333–1344. [PubMed: 21233488]
32. Britt JP, McDevitt RA, Bonci A. Use of channelrhodopsin for activation of CNS neurons. Curr Protoc Neurosci. 2012 Chapter 2, Unit2 16.
33. Qi J, et al. A glutamatergic reward input from the dorsal raphe to ventral tegmental area dopamine neurons. Nat Commun. 2014; 5:5390. [PubMed: 25388237]
34. Root DH, Mejias-Aponte CA, Qi J, Morales M. Role of glutamatergic projections from ventral tegmental area to lateral habenula in aversive conditioning. J Neurosci. 2014; 34:13906–13910. [PubMed: 25319687]

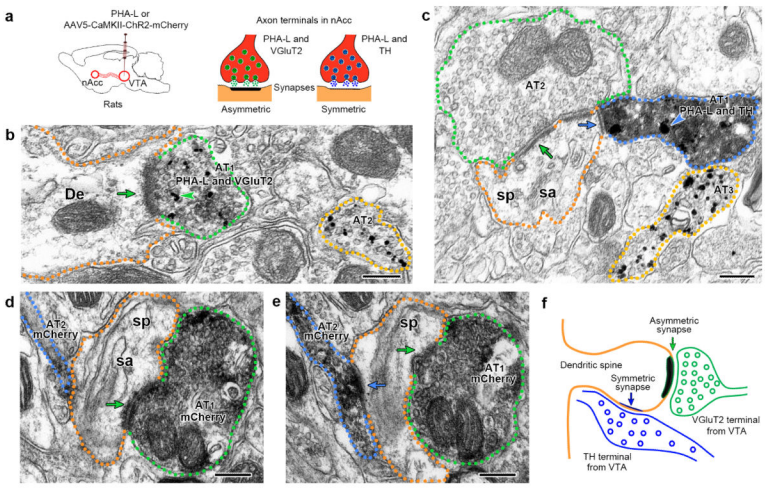

Figure 1. Mesoaccumbens neurons establish either VGluT2-asymmetric synapses or TH-symmetric synapses (wild type rats)

(a) VTA inputs to nAcc identified by PHA-L- or mCherry-immunoreactivity (IR). VTA neurons were tagged with PHA-L (n = 3) or AAV5-CaMKII-ChR2-mCherry (n = 2). Within the nAcc, PHA-L-IR axon terminals make asymmetric or symmetric synapses on dendrites or dendritic spines.

(b) nAcc axon terminal 1 (AT_1, green outline) co-expressing PHA-L-IR (scattered dark material) and VGluT2-IR (gold particles, green arrowhead) makes an asymmetric synapse (green arrow) with a dendrite (De, orange outline). AT_2 (yellow outline) contains only VGluT2-IR.

(c) nAcc AT_1 (blue outline) co-expressing PHA-L-IR (scattered dark material) and TH-IR (gold particles, blue arrowhead) makes a symmetric synapse (blue arrow) on the side of a dendritic spine (sp, orange outline) with spine apparatus (sa). The head of this dendritic spine also makes an asymmetric synapse (green arrow) with the unlabeled AT_2 (green outline). AT_3 (yellow outline) has only TH-IR.

(d-f) Triad arrangement in which ATs from VTA neurons are converging on the same dendritic spine and establishing different types of synapses. Serial sections of two ATs from VTA neurons expressing mCherry-IR (scattered dark material) under the control of the CaMKII promoter (d and e). Both ATs are making synapses on the same dendritic spine (sp, orange outline); AT_1 (green outline) makes an asymmetric synapse (green arrow) on the head of the spine and AT_2 (blue outline) makes a symmetric synapse (blue arrow) on the side of the same dendritic spine.

Bars: (b, c, d, and e) 200 nm.

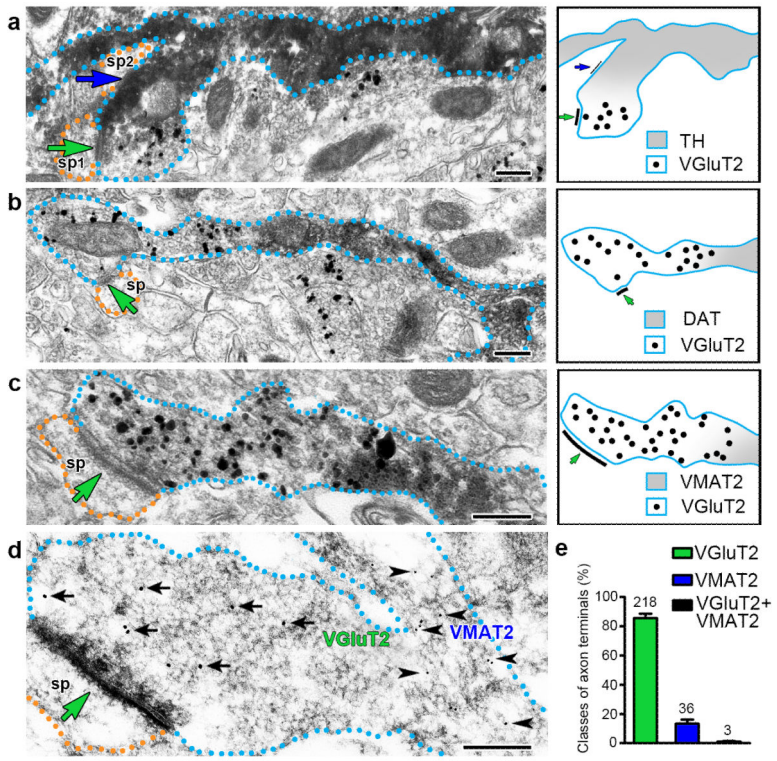

Figure 2. Mesoaccumbens axons from *VGluT2-TH* neurons segregate dopaminergic markers and VGluT2 to different micro-domains (wild type rats)

(a-c) Pre-embedding detection of VGluT2-IR in axon terminals lacking dopaminergic markers, which establish asymmetric synapses (green arrows) on dendritic spines (orange outlines). The VGluT2-IR (gold particles) is confined to the axon terminals. The contiguous axon segments to these VGluT2 terminals contain TH-IR (scattered dark material in a), DAT-IR (scattered dark material in b) or VMAT2-IR (scattered dark material in c). Note that the axon containing TH-IR establishes a symmetric synapse (blue arrow in a). ATs were quantified from the nAcc of rats (n = 4).

(d) Post-embedding detection of VGluT2-IR (18 nm gold particles, black arrows) in an axon terminal lacking VMAT2-IR and establishing an asymmetric synapse (green arrow) on a dendritic spine (orange outline). The contiguous axon segment to this VGluT2-IR terminal contains VMAT2-IR (12 nm gold particles, black arrowheads).

(e) Bars indicating the frequency (mean + s.e.m.) of axon terminals (ATs) containing VGluT2-IR or VMAT2-IR from a total of 257 ATs. Out of these ATs, 85.48 ± 3.03% have VGluT2-IR; 13.37 ± 2.78% have VMAT2-IR and 1.15 ± 0.40% appear to co-express VGluT2-IR and VMAT2-IR (paired t-test, $t(3) = 12.42$, $p = 0.0011$). ATs were quantified from the nAcc of rats (n = 4).

Bars: (a, b, c, and d) 200 nm.

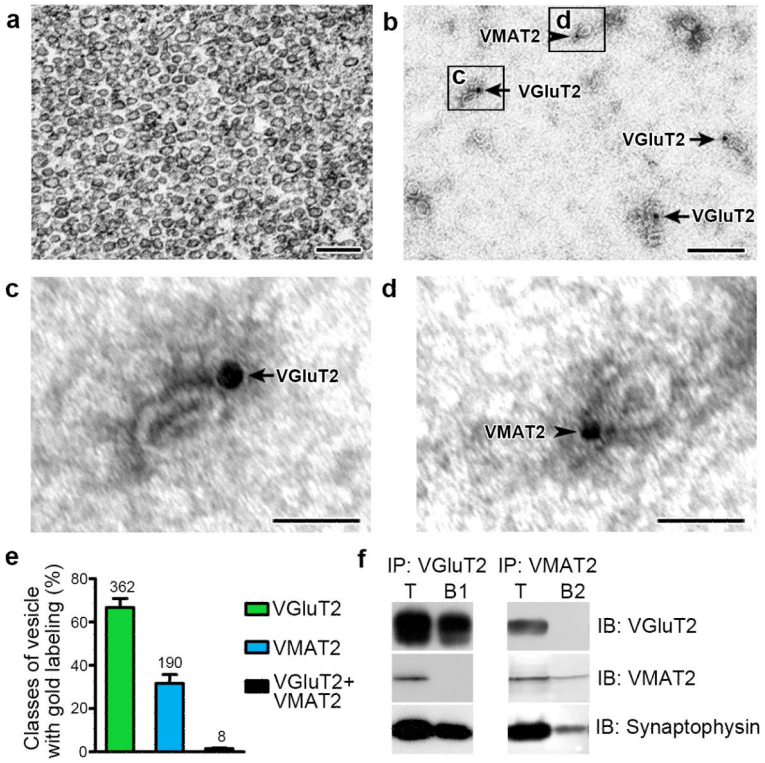

Figure 3. VGluT2 and VMAT2 localize to distinct subpopulations of synaptic vesicles (wild type rats)

(a) Electron micrograph showing the purity and integraty of nAcc isolated synaptic vesicles used for either dual detection of VGluT2-IR and VMAT2-IR (b-d) or co-immunoprecipitation of VGluT2 and VMAT2 (f).

(b-d) Detection of VGluT2-IR (arrows; 18 nm gold particles) or VMAT2-IR (arrowheads; 12 nm gold particles) associated to purified synaptic vesicles.

(e) Bars indicating the frequency (mean + s.e.m.) of vesicles containing VGluT2-IR or VMAT2-IR from a total of 560 labeled vesicles. Out of these vesicles, 66.74 ± 4.10% have VGluT2-IR; 31.71 ± 3.99% have VMAT2-IR and 1.55 ± 0.35% appear to co-label for VGluT2 and VMAT2 (paired t-test, $t(2) = 4.333$, $p = 0.0493$). Synaptic vesicles were quantified from 3 different preparations of isolated vesicles from the nAcc of rats (n = 110).

(f) Western blots of proteins from isolated vesicles prior to immunoprecipitation, IP (T), and after IP with antibodies against VGluT2 (IP:VGluT2; B1) or VMAT2 (IP:VMAT2; B2). Western blots were immunolabeled (IB) with antibodies against VGluT2, VMAT2 or the vesicular marker synaptophysin. The vesicular nature of each fraction was confirmed by the detection of synaptophysin. VGluT2 and VMAT2 are present in the total pool of vesicles (T). In contrast, VGluT2 is detected only in the sample IP with anti-VGluT2 antibodies (IP:VGluT2), and VMAT2 is detected only in the sample IP with anti-VMAT2 antibodies. The western blots were successfully repeated at least 3 times. Full-length blots are presented in Supplementary Figure 3.

Bars: (a and b) 200 nm; (c and d) 50 nm.

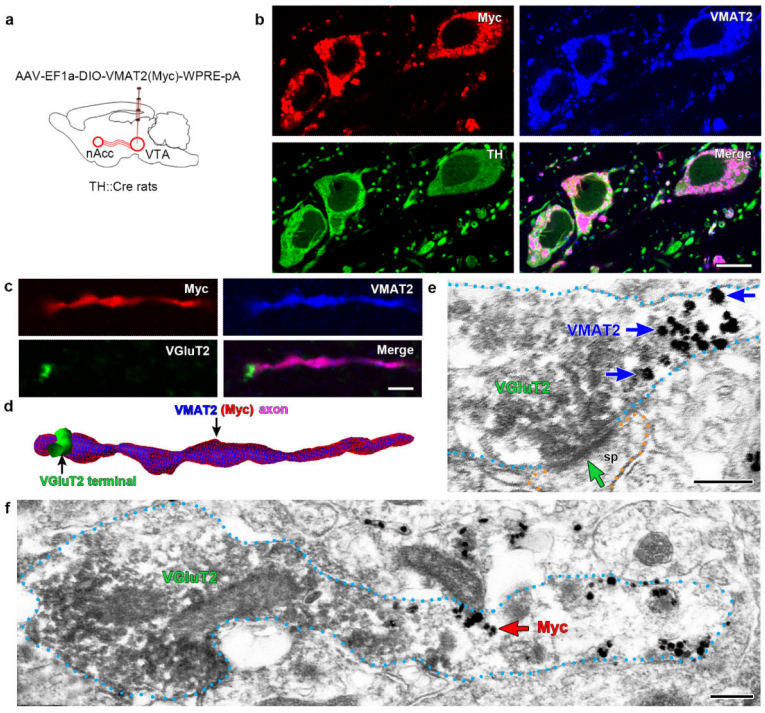

Figure 4. Subcellular segregation of VGluT2-IR and VMAT2(Myc)-IR within the same VGluT2-TH axon from a TH::Cre rat overexpressing VMAT2(Myc) under the regulation of the TH-promoter [TH-VMAT2(Myc) rats]

(a) Schematic representation of VTA inputs (identified by Myc and VMAT2 content) to nAcc. VGluT2-TH and TH-only neurons were infected by injections of AAV-EF1a-DIO-VMAT2(Myc)-WPRE-pA into the VTA of TH::Cre rats [TH-VMAT2(Myc) rats, n = 4].

(b) Immunofluorescence detection of Myc-IR (red), VMAT2-IR (blue), and TH-IR (green) in the medial VTA. Myc-IR, VMAT2-IR, and TH-IR are seen in the same cell bodies and processes.

(c-d) Immunofluorescence detection of Myc-IR (red), VMAT2-IR (blue), and VGluT2-IR (green) in the nAcc. (c) Myc-IR and VMAT2-IR are present in the same axon, but VGluT2-IR is restricted to a terminal-like structure lacking both Myc-IR and VMAT2-IR. (d) The VGluT2-IR terminal-like structure in continuum to an axon co-expressing Myc-IR and VMAT2-IR is better seen in this 3-D reconstruction from Z-stack confocal microscopy images.

(e-f) Electron micrographs of ATs containing VGluT2-IR (scattered dark material), but lacking both VMAT2-IR and Myc-IR (gold particles). The VGluT2-IR axon-terminal is adjacent to an axon segment that contains VMAT2-IR (blue arrow, gold particles in e) or Myc-IR (red arrows, gold particles in f). Note in e that the axon-terminal containing VGluT2-IR establishes an asymmetric synapse (green arrow).

Bars: (b) 10 μm; (c) 2 μm; and (e and f) 200 nm.

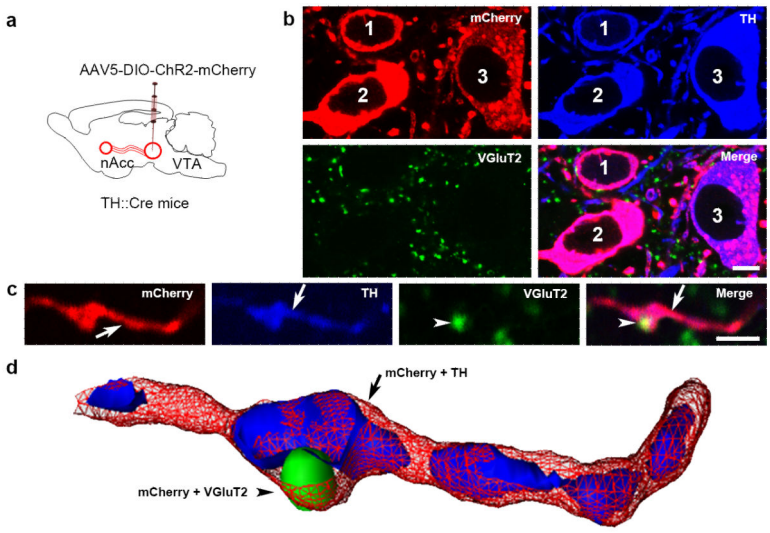

Figure 5. *VGluT2-TH* neurons segregate VGluT2-IR and TH-IR to distinct subcellular compartments within the same axon (TH::Cre mice)

(a) Schematic representation of nAcc inputs from VTA neurons expressing mCherry-IR under the regulation of TH-promoter (TH-ChR2-mCherry mice, n = 4).

(b-d) Fluorescence detection of mCherry-IR (red), TH-IR (blue), and VGluT2-IR (green) in the lateral VTA and nAcc. (b) Within the VTA, mCherry-IR is seen in cell bodies (1, 2, and 3) and processes. These mCherry-IR cell bodies lack VGluT2-IR, but have TH-IR. Within the nAcc, mCherry (under the regulation of the TH-promoter) is detected throughout the axon (red in c). In contrast, VGluT2-IR is restricted to a terminal-like structure (arrowheads in c). TH-IR is present in segments within the mCherry-IR axon (arrow in c). (d) Segregation among one VGluT2 terminal-like structures and TH-axon segments within the same nAcc axon from a *VGluT2-TH* neuron is better seen in this 3-D reconstruction from Z-stack confocal microscopy images of triple labeled nAcc .

Bars: (b) 5 μm; and (c) 2 μm.

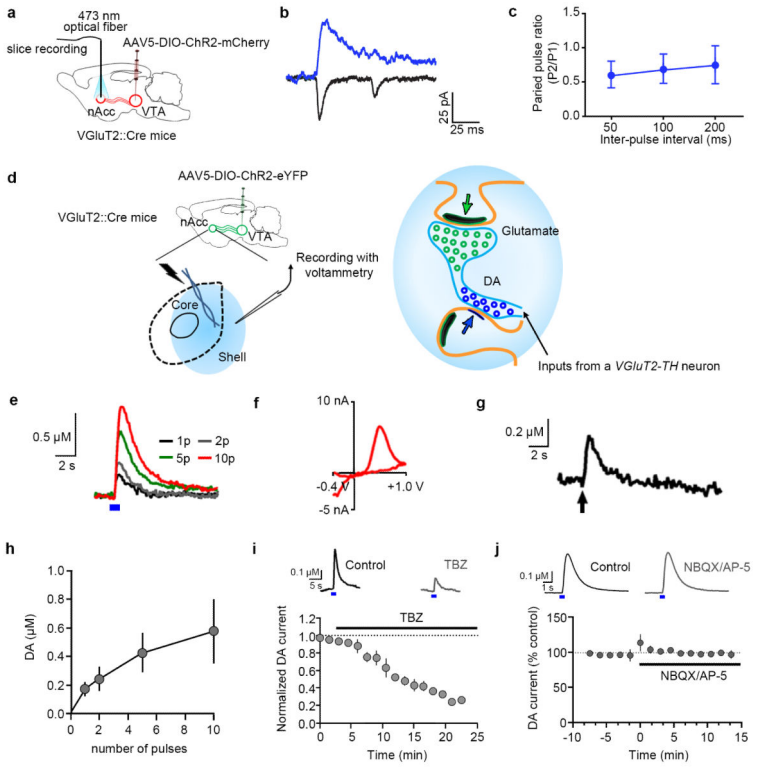

Figure 6. Photo-stimulation of mesoaccumbens VGluT2 fibers expressing ChR2 under the control of the VGluT2 promoter elicits EPSCs and dopamine release in nAcc (VGluT2::Cre mice)

(a-c) Photo-stimulation of nAcc fibers from VGluT2 VTA neurons (n = 6 VGluT2-ChR2-mCherry mice). (b) Optically-evoked EPSCs recorded in nAcc shell. (c) Paired pulse ratios (P2/P1) in nAcc neurons (n = 9 per time point).

(d) Electrically- or optically-evoked dopamine were measured by voltammetry. (e) Optically-evoked dopamine release was increased in response to the increment of the number of pulses; 5 ms pulses (blue box) at 25 Hz. (f) dopamine voltammogram in response to 10 pulses of photo-stimulation. (g) Electrically-evoked dopamine release (10 × 1 ms pulses at 25 Hz; arrow) at the same location of photo-stimulation. (h) Summary of dopamine release in response to the number of optical pulses (n = 6 slices from 3 mice). (i) Bath application of the VMAT2 inhibitor tetrabenazine (TBZ, 10 µM) significantly reduced optically-evoked dopamine release ($p = 0.02$ vs control, paired t-test, n = 4 slices from 2 mice). (j) optically-evoked dopamine responses from *VGluT2-TH* neurons are not dependent on glutamate receptors. Traces show optically-evoked (25 Hz, 5 pulses, 5 ms) nAcc voltammetric currents measured prior to and following application of the glutamate receptor antagonists NBQX (5µM) and AP-5 (40 µM). Graph shows the time course summary (mean ± s.e.m., n = 4 recordings from 2 mice); NBQX and AP-5 were applied during the time indicated by the bar. No significant effect on the dopamine signals was observed (two-tailed paired t-test, $t(3) = 0.1239$, $p = 0.9093$).